Thinning $CsPb_2Br_5$ perovskite down to monolayers: Cs-dependent stability

F. Iyikanat,[1,*] E. Sari,[2] and H. Sahin[2,3,†]

[1]*Department of Physics, Izmir Institute of Technology, 35430 Izmir, Turkey*

[2]*Department of Photonics, Izmir Institute of Technology, 35430 Izmir, Turkey*

[3]*ICTP-ECAR Eurasian Center for Advanced Research, Izmir Institute of Technology, 35430 Izmir, Turkey*

(Received 4 May 2017; revised manuscript received 24 July 2017; published 19 October 2017)

Using first-principles density functional theory calculations, we systematically investigate the structural, electronic, and vibrational properties of bulk and potential single-layer structures of perovskitelike $CsPb_2Br_5$ crystal. It is found that while Cs atoms have no effect on the electronic structure, their presence is essential for the formation of stable $CsPb_2Br_5$ crystals. The calculated vibrational spectra of the crystal reveal that not only the bulk form but also the single-layer forms of $CsPb_2Br_5$ are dynamically stable. Predicted single-layer forms can exhibit either semiconducting or metallic character. Moreover, the modification of the structural, electronic, and magnetic properties of single-layer $CsPb_2Br_5$ upon formation of vacancy defects is investigated. It is found that the formation of Br vacancy (i) has the lowest formation energy, (ii) significantly changes the electronic structure, and (iii) leads to ferromagnetic ground state in the single-layer $CsPb_2Br_5$. However, the formation of Pb and Cs vacancies leads to *p*-type doping of the single-layer structure. Results reported herein reveal that the single-layer $CsPb_2Br_5$ crystal is a novel stable perovskite with enhanced functionality and a promising candidate for nanodevice applications.

DOI: 10.1103/PhysRevB.96.155442

I. INTRODUCTION

In recent years, hybrid organic-inorganic lead halide perovskites have attracted immense interest because of their low cost, easy fabrication, and superior optoelectronic properties [1,2]. These hybrid perovskites exhibit great potential in device applications such as photodetectors [3], laser devices [4], flexible solar cells [5], and light emitting diodes (LEDs) [6,7]. One of the most studied organic-inorganic hybrid perovskites is $CH_3NH_3PbX_3$ (where X = Cl, Br, or I). Noh *et al.* showed that the band gap of $CH_3NH_3Pb(I_{1-x}Br_x)$ can be controlled by composition engineering and the absorption edge of the mixed halide perovskite can be altered in a controlled manner to cover almost the whole visible spectrum [8]. It was also demonstrated that organic-inorganic hybrid perovskites exhibit high power conversion efficiency of exceeding 20% [9,10]. The fully inorganic $CsPbX_3$ (X = Cl, Br, or I) exhibits higher chemical stability and excellent optoelectronic properties compared to organic-inorganic perovskites [11–13]. It was found that these all-inorganic materials exhibit extremely high fluorescence quantum yield, very narrow emission bandwidth, and suppressed fluorescence blinking [14,15]. It was shown that $CsPbBr_3$ exhibits high carrier mobility and large diffusion length [16]. It has been theoretically predicted that $CsPbBr_3$ is highly defect-tolerant in terms of its electronic structure [17].

After successful isolation of graphene monolayers from bulk graphite, research on ultra-thin 2D crystal structures has experienced a remarkable growth [18]. It has been demonstrated by many groups that quantum effects that emerge as a consequence of dimensional reduction may lead to novel features in low-dimensional materials [19,20]. The rapid progress in the synthesis and fabrication methods of 2D materials has not only led to exploration of graphenelike materials but also monolayer 2D hybrid perovskites. It was reported that the thickness and photoluminescence emission of hybrid perovskite nanoplatelets can be controlled by varying the ratio of the organic cations used [21]. Recently, atomically thin organic-inorganic hybrid perovskites synthesized with efficient photoluminescence and modulation of color have been achieved by tuning the thickness and composition of the crystal [22]. The synthesis of layered $CH_3NH_3PbX_3$ (where X = Cl, Br, or I) down to a thickness of a few unit cells and even single unit-cell layers were accomplished by a combined solution process and vapor-phase conversion method [23]. It was found that by controlling the atomic ratio of the halide anions, the stability of the hybrid perovskites can be improved [8]. Compared to organic-inorganic hybrid perovskites, all-inorganic perovskites, in which cesium ions replace organic cations, exhibit higher chemical stability [12,24]. However, the low environmental stability of hybrid organic-inorganic perovskites is a crucial issue that needs to be addressed for potential future applications.

Moreover, all-inorganic $CsPb_2Br_5$ emerged as a 2D version of lead halide perovskite materials. $CsPb_2Br_5$ has a tetragonal phase which consists of alternating Cs^+ and $[Pb_2Br_5]^-$ polyhedron layers. Theoretical and experimental investigations showed that $CsPb_2Br_5$ is an indirect band gap semiconductor with a band gap of 2.98 eV [25] Large-scale synthesis of highly luminescent $CsPb_2Br_5$ nanoplatelets was already reported [26]. It was found that a dual phase of $CsPbBr_3$-$CsPb_2Br_5$ exhibits increased conductivity and improved emission life time compared to that of the pure $CsPbBr_3$ [27]. However, the thickness and composition dependent structural stability and electronic properties of $CsPb_2Br_5$ remain almost unexplored. It is known that ultrathin 2D materials are more sensitive to environmental conditions than their bulk counterparts. Environmental conditions and substrate can affect the structural stability and characteristic properties of ultrathin 2D materials. It was reported that in the presence of chlorine, when $CH_3NH_3PbI_3$ films are deposited on a TiO_2 mesoporous layer,

*fadiliyikanat@iyte.edu.tr

†hasansahin@iyte.edu.tr

a stable cubic phase is formed in $CH_3NH_3PbI_3$ perovskite, instead of the commonly observed tetragonal phase [28]. In a recent study, $CsPb_2Br_5$ nanosheets were obtained via an oriented attachment of $CsPbBr_3$ nanocubes [25]. It was also reported that inorganic Cs atom plays a significant role in the stability of perovskites [29,30]. The Cs atom as a cation, donates charge to the lattice of a perovskite and fulfill the charge neutrality.

Although the bulk forms of many perovskites have been studied intensely, the effect of dimensional reduction in the characteristic properties of $CsPb_2Br_5$ crystal has not been investigated before. In the current study, using first-principles calculations based on density functional theory (DFT), we present a detailed analysis of the structural, electronic, vibrational, and vacancy-dependent characteristics of single-layer $CsPb_2Br_5$. The paper is organized as follows. Details of the computational methodology are given in Sec. II. Structural and electronic properties of bulk $CsPb_2Br_5$ are given in Sec. III. The effect of dimensional crossover on the structure and electronic properties of $CsPb_2Br_5$ crystal is presented in Sec. IV. Structural, electronic, and magnetic properties of various vacancy defects are discussed in Sec. V. We conclude our results in Sec. VI.

II. COMPUTATIONAL METHODOLOGY

All the calculations were performed using the projector augmented wave (PAW) [31,32] potentials as implemented in the Vienna *ab initio* simulation package (VASP) [33,34]. The local density approximation (LDA) [35] was used with the inclusion of spin-orbit coupling (SOC) to describe the exchange and correlation potential as parametrized by the Ceperley and Alder functional [36]. To obtain the partial charge on the atoms, the Bader technique was used [37].

A plane-wave basis set with kinetic energy cutoff of 500 eV was used for all the calculations. The total energy difference between the sequential steps in the iterations was taken as 10^{-5} eV as a convergence criterion. The total force in the unit cell was reduced to a value of less than 10^{-4} eV/Å. For bulk and single-layer $CsPb_2Br_5$, Γ-centered k-point meshes of $4 \times 4 \times 3$ and $4 \times 4 \times 1$ were used, respectively. In order to model single-layer $CsPb_2Br_5$, a vacuum spacing larger than 14 Å was inserted to avoid spurious interactions between adjacent layers. Dipole corrections were applied in the direction perpendicular to the plane of the charged monolayers [38]. Gaussian smearing of 0.05 eV was used for electronic density of states calculations. The cohesive energy per atom was formulated as

$$E_{\text{coh}} = \left(\sum n_a E_a - E_{\text{Str}}\right)/N, \quad (1)$$

where E_a denotes the energy of a single isolated atom and n_a denotes the number of corresponding atoms contained in the unit cell. E_{Str} denotes the total energy of the structure. N denotes the number of total atoms contained in the unit cell. Phonon calculations were performed by making use of the small displacement method as implemented in the PHON software package [39]. Out-of plane acoustic phonon modes in $CsPb_4Br_{10}$, ss-$CsPb_2Br_5$, and ds-$CsPb_2Br_5$ crystal structures are corrected by quadratic-fitting at the vicinity of zone center. (For detailed information, see Ref. [40].)

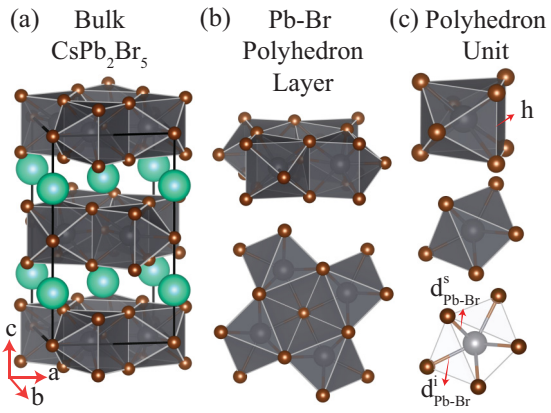

FIG. 1. (a) Tilted side view of bulk $CsPb_2Br_5$. (b) Tilted side and top views of Pb-Br polyhedron layer. (c) Tilted side and top views of Pb-Br polyhedron. Green, brown, and gray balls illustrate Cs, Br, and Pb atoms, respectively.

III. BULK $CsPb_2Br_5$

Before a detailed discussion of the potential single-layer forms of $CsPb_2Br_5$, we first investigate the structural properties of the bulk form of the crystal. The tetragonal phase of $CsPb_2Br_5$ is shown in Fig. 1(a). $CsPb_2Br_5$ consists of a sandwiched structure with alternating Cs and Pb-Br polyhedron layers. The calculated lattice parameters are $a = 8.24$ Å and $c = 14.57$ Å. Tilted side and top views of Pb-Br polyhedron layer are shown in Fig. 1(b). Pb-Br polyhedron layer is composed of Pb-Br polyhedrons, which are formed by putting a triangular prism and two rectangular pyramids together. Tilted side and top views of Pb-Br polyhedron are shown in Fig. 1(c). There are two different bromine atoms in the polyhedron: one of them is located at the surface of Pb-Br polyhedron layer (Br_s) and the other one is located at the inner plane of the layer (Br_i). Br_i is located in the same plane with Pb atoms and it has the Pb-Br bond distance of $d^i_{\text{Pb-Br}} = 3.08$ Å. The bond length between Br_s and Pb atoms is $d^s_{\text{Pb-Br}} = 2.92$ Å. The thickness of Pb-Br polyhedron layer is $h = 3.83$ Å. The distance between Cs and surface Br atoms is $d^s_{\text{Cs-Br}} = 3.53$ Å. It is found that the cohesive energy per atom of $CsPb_2Br_5$ crystal is 3.42 eV.

For detailed investigation of the bondings in $CsPb_2Br_5$, crystal Bader charge analysis is also performed. As given in the Table I, 0.8 and 1.0e charges are donated by each Cs and Pb atoms, respectively. On the other hand, each Br atom receives 0.6e charge. Therefore analysis of the electronic structure reveals that ionic interaction arises between the layers of Cs and Pb-Br skeleton via vertical charge transport from Cs layer to the Pb-Br skeleton. Furthermore, the bond between Pb and Br atoms in the Pb-Br skeleton has also an ionic character. The Cs-terminated surface of $CsPb_2Br_5$ crystal has a low work function of $\Phi = 1.17$ eV.

Figure 2 shows the band structure and projected density of states (PDOS) for $CsPb_2Br_5$ crystal. It can clearly be seen from the figure that bulk $CsPb_2Br_5$ exhibits an indirect band gap,

TABLE I. The calculated ground-state properties for bulk (**b**) $CsPb_2Br_5$ and single-layer Pb_2Br_5, $CsPb_4Br_{10}$, ss-$CsPb_2Br_5$, ds-$CsPb_2Br_5$, and $Cs_2Pb_2Br_5$: the lattice constants in the lateral and vertical directions, a and c, respectively; thickness of the Pb-Br polyhedron layer, h; atomic distances between Pb and Br atoms, $d^i_{\text{Pb-Br}}$ and $d^s_{\text{Pb-Br}}$; atomic distance between Cs and surface Br atoms, $d^s_{\text{Cs-Br}}$; the cohesive energies, E_{coh}; the amount of donated (−) charge by the Br_i, Br_s, Pb, and Cs atoms are $\Delta\rho^i_{\text{Br}}$, $\Delta\rho^s_{\text{Br}}$, $\Delta\rho_{\text{Pb}}$, and $\Delta\rho_{\text{Cs}}$, respectively; the energy band gap of the structure, gap; the work function, Φ.

	a (Å)	c (Å)	h (Å)	$d^i_{\text{Pb-Br}}$ (Å)	$d^s_{\text{Pb-Br}}$ (Å)	$d^s_{\text{Cs-Br}}$ (Å)	E_{coh} (eV)	$\Delta\rho^i_{\text{Br}}$ (e)	$\Delta\rho^s_{\text{Br}}$ (e)	$\Delta\rho_{\text{Pb}}$ (e)	$\Delta\rho_{\text{Cs}}$ (e)	Gap (eV)	Φ (eV)
b $CsPb_2Br_5$	8.24	14.57	3.83	3.08	2.92	3.53	3.42	0.6	0.6	−1.0	−0.8	2.41	1.17
Pb_2Br_5	8.09	-	3.72	3.02	2.88	-	3.08	0.5	0.4	−1.0	-	-	7.00
$CsPb_4Br_{10}$	8.18	-	3.77	3.05, 3.08	2.94	3.44	3.21	0.5	0.5	−1.0	−0.8	-	4.53
ss-$CsPb_2Br_5$	8.29	-	3.85	3.11	2.84	3.42	3.31	0.6	0.5	−1.0	−0.8	2.53	2.75
ds-$CsPb_2Br_5$	8.29	-	3.81	3.11	2.92	3.43	3.32	0.6	0.6	−1.0	−0.8	2.54	4.79
$Cs_2Pb_2Br_5$	8.21	-	4.31	3.18	3.22	3.35	3.15	0.6	0.7	−0.8	−0.8	-	1.45

with the valence-band maximum (VBM) residing along the line Γ-X (①), while the conduction-band minimum (CBM) being located at the Γ point (⑤). The indirect gap calculated with LDA+SOC is 2.41 eV. It is known that experimentally observed band gaps, which are underestimated by both bare-LDA and bare-GGA functionals, can be well-approximated by the considering screening (GW calculations) and excitonic (solving Bethe-Salpeter equation) effects. However, due to high computational cost, GW and BSE calculations are not taken into account here. The partial contributions of orbital states to electronic DOS of bulk $CsPb_2Br_5$ crystal are given in Fig. 2(b). It appears that the major contribution to the states around the band edges originates from Pb and Br atoms. While the VBM is dominated by p orbitals of Br atom, the CBM is mostly composed of the p orbitals of Pb atom. The states of the Cs atom reside at deep energy levels, therefore, they have no effect on the electronic structure of the crystal. Band-decomposed charge densities of the valence- and conduction-band edges are also given in the Fig. 2. As seen in the figure, edges on the top of the valence band are composed of the p_x and p_y orbitals of Br_s atoms. Valance-band edges in between Γ and M (②), Z and R (③), A and Z (④) points differ by 23, 53, and 74 meV from the VBM of the single layer, respectively. On the other hand, the top of the conduction-band edges (⑤ and ⑥) is mostly made up of the p_x and p_y orbitals of the Pb atom.

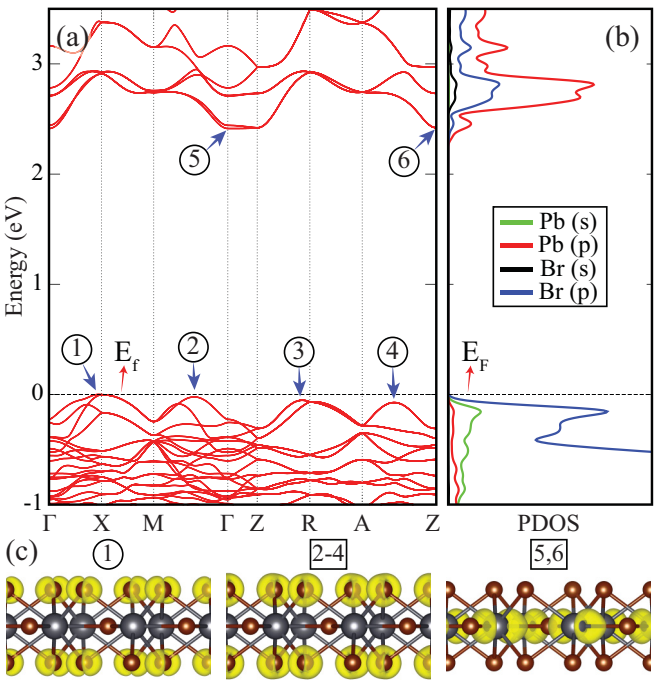

FIG. 2. (a) The energy-band dispersion and (b) partial density of states of bulk $CsPb_2Br_5$. (c) The band decomposed charge densities of the bulk $CsPb_2Br_5$ at the labeled band edges. Isosurface value of charge density is $2 \times 10^{-5}\, e/\text{Å}^3$.

IV. THINNING $CsPb_2Br_5$ DOWN TO MONOLAYERS

In this section, we investigate the possible stable structure of single-layer $CsPb_2Br_5$ crystal and the effect of dimensional crossover on its characteristic properties. Five reasonable single-layer configurations derived from bulk $CsPb_2Br_5$ structure are shown in Fig. 3. According to their chemical compositions, these five structures are named as Pb_2Br_5, $CsPb_4Br_{10}$, single-side Cs terminated $CsPb_2Br_5$ (ss-$CsPb_2Br_5$), double-side Cs terminated $CsPb_2Br_5$ (ds-$CsPb_2Br_5$), and $Cs_2Pb_2Br_5$. Depending on whether the synthesis technique is growth or mechanical exfoliation process one of these of the single-layer crystal structures or their mixtures can be obtained.

Single-layer Pb_2Br_5 is a Cs-free skeleton composed of only Pb-Br polyhedrons. As given in Table I, the calculated lattice parameter and thickness of Pb_2Br_5 are $a = 8.09$ Å and $h = 3.72$ Å, respectively. These values are relatively small compared to those of bulk. The calculated bond lengths between the atoms of the structure are given in the Table I. To assess the dynamical stability, phonon dispersions of single-layer Pb_2Br_5 are calculated and shown in Fig. 3(a). A $3 \times 3 \times 1$ supercell is used for the phonon band structure calculations of single-layer forms of the crystal. The phonon spectra of the structure exhibit imaginary eigenvalues through all the symmetry points, indicating the instability of the structure. Instability in the structure could be attributed to the charge transfer mechanism between ions of the structure. As given in Table I, the resulting charges of Br atoms of Pb_2Br_5 are lower than that of bulk $CsPb_2Br_5$. Although each Pb atom donates $1.0e$ charge, each Br_i and Br_s atoms receive 0.5 and $0.4e$ charges, respectively. Therefore unsaturated Br_i and Br_s atoms may lead to dynamical instability in single-layer Pb_2Br_5.

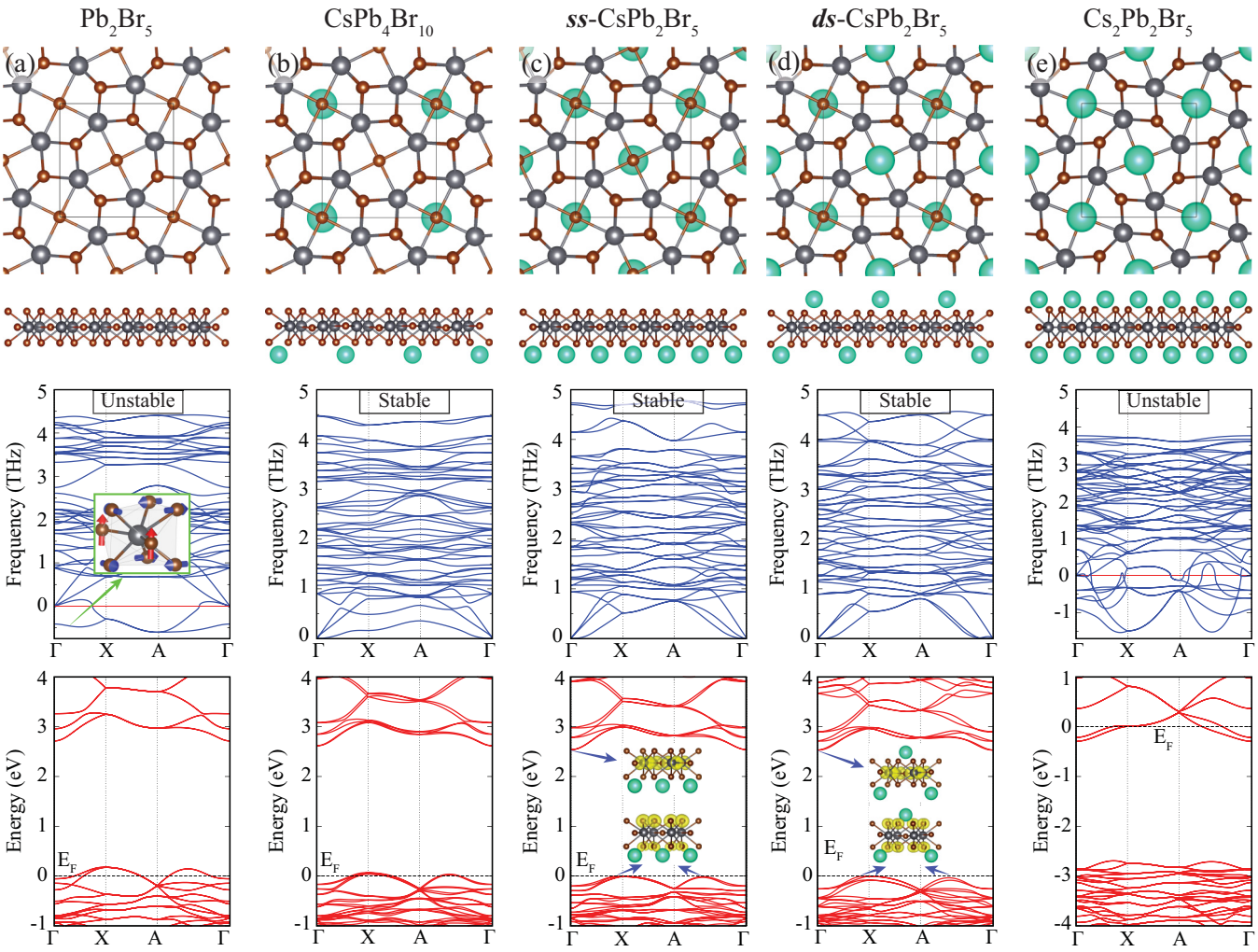

FIG. 3. Possible single-layer structures of $CsPb_2Br_5$ crystal. Top and side views of the structures, phonon spectrum, and SOC included electronic band diagrams of single-layer (a) Pb_2Br_5 (inset: tilted side view of atomic displacements of the corresponding mode), (b) $CsPb_4Br_{10}$, (c) *ss*-$CsPb_2Br_5$, (d) *ds*-$CsPb_2Br_5$, and (e) $Cs_2Pb_2Br_5$. Isosurface value of band decomposed charge densities (inset of band structure of *ss*-$CsPb_2Br_5$) is $2 \times 10^{-5}\, e/\text{Å}^3$.

For a deeper analysis of instability of single-layer Pb_2Br_5, atomic displacements of the lowest mode are shown in the inset of phonon band diagram of Fig. 3(a). It appears that the mode responsible for the instability of the structure is due to vibrations of Br_i and Br_s atoms normal and parallel to the plane of the structure, respectively. Imaginary eigenfrequencies in the whole Brillouin zone indicate the lack of required restoring force against these atomic motions. Therefore the structure is unstable under this motion and transforms to another phase. This instability can be cured by increasing the bond strength between Pb and Br atoms through adding extra charges.

As shown in Fig. 3(b), a single-layer of $CsPb_4Br_{10}$ is formed through half of the single-side of Pb-Br layer covered by Cs atoms. The lattice parameter and the thickness of the structure are $a = 8.18$ Å and $h = 3.77$ Å, respectively. It is found that the single-layer $CsPb_4Br_{10}$ is formed by a cohesive energy of 3.21 eV. Since one side of the structure is covered by Cs atoms, the bonds show anisotropy in the vertical direction (see Table I). Given values of the bond lengths belong to the Cs terminated side of the structure. The phonon spectra of single-layer $CsPb_4Br_{10}$ exhibit real eigenvalues through all the symmetry points, confirming the dynamical stability of the layers. Bader charge analysis shows that Cs and Pb atoms of the structure donate 0.8 and 1.0*e* charges, respectively. Therefore the amount of received charges by each Br atom is 0.5*e*. The work function of the structure is calculated to be 4.53 eV. It is also seen from Fig. 3(b) that lowering the concentration of Cs atoms leads to unfilling of the valence-band edge and therefore *p*-type conductivity in the single-layer $CsPb_4Br_{10}$.

Relaxed geometric structures of *ss*-$CsPb_2Br_5$ and *ds*-$CsPb_2Br_5$ are shown in Figs. 3(c) and 3(d), respectively. These two structures possess the same chemical composition with the $CsPb_2Br_5$ crystal. The lattice parameters of both of the structures are $a = 8.29$ Å. The thickness of the Pb_2Br_5 sublayer of *ss*-$CsPb_2Br_5$ and *ds*-$CsPb_2Br_5$ are $h = 3.85$ and 3.81 Å, respectively. As given in Table I, the atom-atom bond distances of these two structures are very similar to that of the bulk $CsPb_2Br_5$. Real frequencies in the phonon spectra of single-layer structures [Figs. 3(c) and 3(d)] of *ss*-$CsPb_2Br_5$ and *ds*-$CsPb_2Br_5$ appear in a whole Brillouin zone, indicating

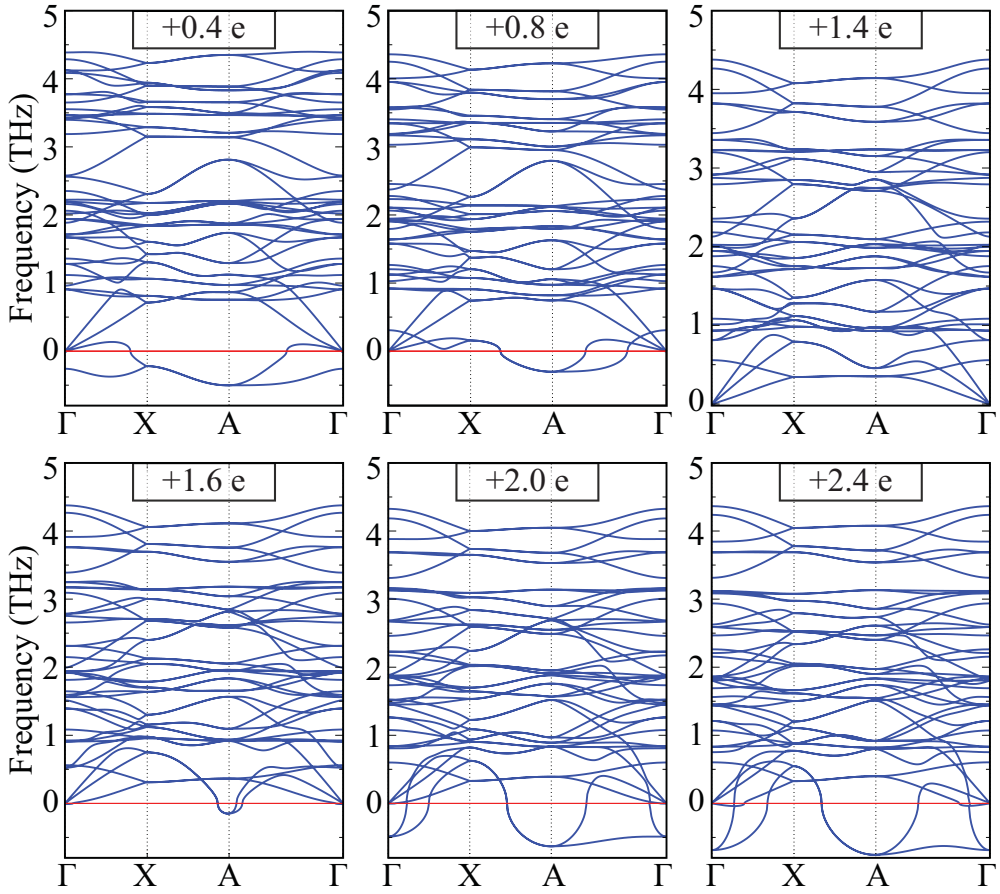

FIG. 4. Charging-dependent phonon dispersion of single-layer skeleton structure of Pb_2Br_5.

the dynamical stabilities of these two structures. Bader charge analysis reveals that the charge transfer mechanism of single layers of ss-$CsPb_2Br_5$ and ds-$CsPb_2Br_5$ are very similar to the bulk $CsPb_2Br_5$. Cs and Pb atoms of both structures donate 0.8 and 1.0e charges, respectively. The amount of charge received by Br atoms of the two structures are in the range of 0.5–0.6e. Therefore Pb-Br skeletons of the two structures are saturated with enough charges to maintain stable bonding mechanism. In addition, cohesive energies of these two structures are given in Table I. Among the single-layer forms of the crystal, due to the vertical symmetry and the same chemical composition with the bulk counterpart, ds-$CsPb_2Br_5$ has the highest cohesive energy. Furthermore, the calculated work function values of singe-layers of ss-$CsPb_2Br_5$ and ds-$CsPb_2Br_5$ are 2.75 and 4.79 eV, respectively. The calculated values of the work functions belong to the Cs-terminated side of the structure. Hence the work function shows a decreasing behavior with increasing concentration of Cs atoms of the Cs-terminated side. As shown in Figs. 3(c) and 3(d), single-layer ss-$CsPb_2Br_5$ and ds-$CsPb_2Br_5$ have very similar electronic band diagrams and they are indirect band gap semiconductors. The VBMs of the two structures reside at X point, whereas their CBMs reside at Γ point. It is worth mentioning that the valence-band edge in between A and Γ points differs only by 24 meV energy from the VBM of the two structures. The band-decomposed charge densities at the valence-band and the conduction-band edges of the two structures are shown in Figs. 3(c) and 3(d). Band edge characteristics of these structures possess very similar behavior with their bulk counterpart. As given in Table I, the SOC included band gap of ss-$CsPb_2Br_5$ and ds-$CsPb_2Br_5$ are 2.53 and 2.54 eV, therefore, with decreasing thickness from bulk to single layer, the band gap of $CsPb_2Br_5$ increases by ∼0.13 eV.

The single-layer $Cs_2Pb_2Br_5$ is constructed by three submonolayers: a Pb_2Br_5 sublayer and two surrounding sublayers of Cs atoms. The calculated lattice parameter of $Cs_2Pb_2Br_5$, $a = 8.21$ Å, is very similar to the bulk lattice parameter of the crystal. However, the thickness of Pb_2Br_5 sublayer is $h = 4.31$ Å, which is much higher than that of the other single-layer forms of the crystal. As in Pb_2Br_5, phonon spectra of single-layer $Cs_2Pb_2Br_5$, shown in Fig. 3(e), exhibit imaginary eigenvalues through all the symmetry points, indicating the dynamical instability of the structure. In single-layer $Cs_2Pb_2Br_5$, while each Cs and Pb atom donate 0.8e charges, each Br_i and Br_s atoms receive 0.6 and 0.7e charges, respectively. Extra charges provided by Cs atoms lead to a decrease in charge transfer between Pb and Br atoms. Therefore the Cs-induced weakening of the Pb-Br bonds is the reason of the instability in the single-layer $Cs_2Pb_2Br_5$.

Effect of Cs atoms via the charging of Pb_2Br_5 skeleton

In this chapter, in order to facilitate a deeper understanding of the role of Cs atoms, we examine the stability of Cs-free

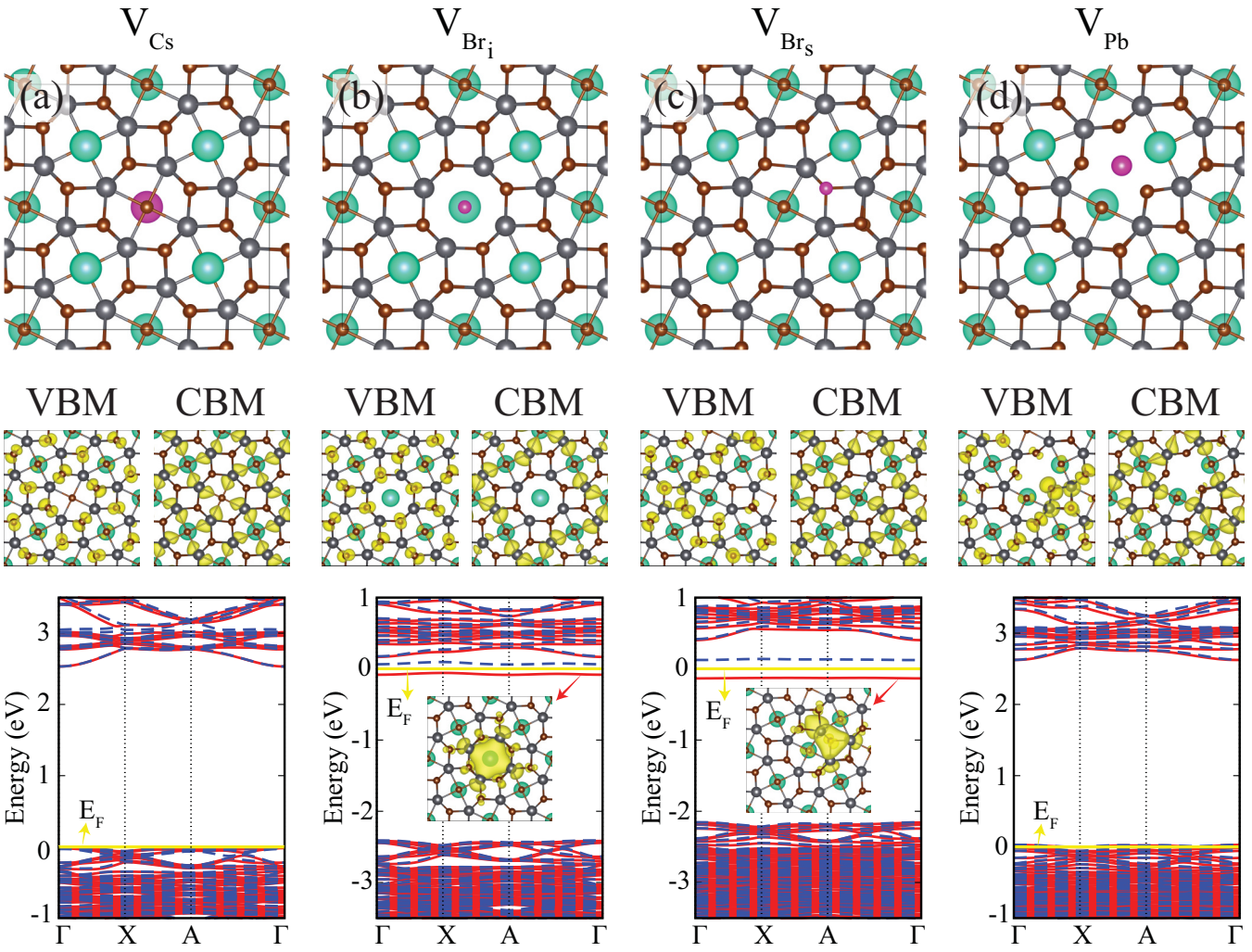

FIG. 5. Top view of the structures, band decomposed charge densities of the VBM and CBM, and electronic band structures of single-layer *ds*-$CsPb_2Br_5$ with (a) Cs vacancy, (b) Br_i vacancy, (c) Br_s vacancy, and (d) Pb vacancy. Pink atoms illustrate removed atoms. Yellow, red, and dashed blue lines in band diagrams illustrate the Fermi level, majority, and minority spin bands, respectively. Band decomposed charge densities of in-gap states of V_{Br_i} and V_{Br_s} are shown in the insets of the corresponding band diagrams. Isosurface value of charge density is $6 \times 10^{-6}\, e/\text{Å}^3$.

Pb_2Br_5, which is already presented to be unstable in the previous chapter, via charging calculations. One low-lying optical and one acoustic phonon branch that have imaginary eigenfrequencies are the direct indication of dynamical instability in the single-layer structure of Cs-free Pb_2Br_5. However, as calculated in the previous chapter, the single-layer skeleton structure of Pb_2Br_5 can be stabilized through the adsorption of Cs atoms. Therefore a question arises as to whether or not the stability of $CsPb_2Br_5$ is provided only by the charge transferred from Cs atoms to Pb_2Br_5 skeleton.

As shown in Fig. 4, the role of electron transfer on the stability of Pb_2Br_5 can be examined through the addition of extra electrons into the primitive unit cell. Here, it is important to note that once the unit cell is charged by extra electrons, the structure is re-optimized by considering that the new charge distribution and phonon calculations are performed for this fully relaxed structure. Figure 4 shows that one acoustic and one low-lying optical branches, having imaginary eigenfrequencies, of the Pb_2Br_5 skeleton can be fixed upon charging. It appears that while the structure is fully stabilized under 1.4 *e* charging, it exhibits instability under over-charged and less-charged situations. Therefore it can be concluded that Cs atoms play an important role as a stabilizer of the Pb_2Br_5 skeleton by charge transfer. Such a charge-dependent stability may pave the way to synthesize novel Cs-free perovskite structures and to fix the vacancy-dependent instabilities in similar structures.

V. VACANCY DEFECTS IN SINGLE-LAYER $CsPb_2Br_5$

During the growth or exfoliation of layered crystals, existence of various lattice imperfections is inevitable. One of the most common lattice imperfections in layered crystals is vacancies. The formation of vacancies in ionically bonded materials are the source of trap states and profoundly alter the electronic and optical properties of semiconductors. Therefore it is important to investigate how vacancies are formed and what are the characteristic features. In this section, four

TABLE II. The lattice constants a; formation energies E_{form}; magnetic moments M; electronic characteristics and band gaps of four different defected forms of the $2 \times 2 \times 1$ supercell of the single-layer $CsPb_2Br_5$.

	a (Å)	E_{form} (eV)	M (μ_B)	Electronic characteristic	Band gap (eV)
V_{Cs}	16.48	4.82	0.0	semiconductor	2.53
V_{Br_i}	16.44	5.02	1.0	semiconductor	0.12
V_{Br_s}	16.48	4.51	1.0	semiconductor	0.25
V_{Pb}	16.46	8.20	0.0	metal	-

different vacancy types in single-layer ds-$CsPb_2Br_5$ that correspond to the energetically most favorable structure are considered, Cs vacancy (V_{Cs}), Br_i vacancy (V_{Br_i}), Br_s vacancy (V_{Br_s}), and Pb vacancy (V_{Pb}). In order to hinder the interaction between vacancies in adjacent cells, a 64-atom supercell was used. Relative stabilities of the four vacancies are calculated according to the formula

$$E_{\text{form}} = E_{\text{SL+vac}} + E_A - E_{\text{SL}}, \tag{2}$$

where E_{form} is the formation energy of the relevant vacancy, $E_{\text{SL+vac}}$ is the total energy of the supercell with vacancy, E_A is the isolated-single-atom energy of the removed atom, and E_{SL} is the total energy of the supercell of a single layer.

Relaxed geometric structures when a single Cs, Br_i, Br_s, and Pb are created in the ds-$CsPb_2Br_5$ are shown in Figs. 5(a)–5(d), respectively. Formation of these vacancies leads to negligible distortion on the single-layer ds-$CsPb_2Br_5$. As given in Table II, the fully relaxed lattice parameters of V_{Cs}, V_{Br_i}, V_{Br_s} and V_{Pb} are 16.48, 16.44, 16.48, and 16.46 Å, respectively. The formation of Pb vacancy (V_{Pb}) leads to minor local reconstructions. When a Pb vacancy is introduced, the closest Br atoms to the extracted Pb atom are released and they move toward the neighboring Pb atoms. The formation energies of V_{Cs}, V_{Br_i}, V_{Br_s}, and V_{Pb} are calculated to be 4.82, 5.02, 4.51, and 8.20 eV, respectively. Therefore one can conclude that the formation of Cs and Br vacancies in single-layer ds-$CsPb_2Br_5$ perovskites are more likely.

The electronic band structures of ds-$CsPb_2Br_5$ with V_{Cs}, V_{Br_i}, V_{Br_s}, and V_{Pb} are presented in Figs. 5(a)–5(d), respectively. It appears that the electronic properties of single-layer ds-$CsPb_2Br_5$ do not change significantly with the removal of the Cs atom. Band decomposed charge densities at the valence-band and conduction-band edges of V_{Cs} show similar behavior with that of pristine ds-$CsPb_2Br_5$. Figures 5(b) and 5(c) display band-decomposed charge densities and electronic band diagrams of V_{Br_i} and V_{Br_s}. It is seen that only the formation of Br vacancies leads to presence of in-gap states. Such dispersionless electronic states can be attributed to the unpaired electrons of neighboring Pb and Br atoms. For V_{Br_i} and V_{Br_s} vacancies, two spin-polarized in-gap states are symmetrically placed around the Fermi level with band gaps of 0.12 and 0.25 eV, respectively, which then describe a singly occupied in-gap state with a magnetic moment of 1 μ_B. Figure 5(d) shows that when a Pb vacancy is created, some states of ds-$CsPb_2Br_5$ discharge due to the lack of donor electrons of Pb atom. As a result, the formation of Pb vacancy leads to p-type conductivity in single-layer ds-$CsPb_2Br_5$.

VI. CONCLUSIONS

In conclusion, using first-principles calculations, we investigated the structural, electronic, and vibrational properties of $CsPb_2Br_5$ crystals, and how these properties are affected by dimensional crossover. Bulk $CsPb_2Br_5$ is an indirect band gap semiconductor with a band gap of 2.41 (LDA+SOC) eV. It was calculated that while the valence and conduction-band edges of bulk $CsPb_2Br_5$ crystal are mainly composed of Pb and Br atoms, Cs atoms do not play role in electronic properties.

Then, we predicted that there are two dynamically stable phases of single-layer $CsPb_2Br_5$. These two structures were found to be stable in both total energy optimization and phonon calculations. Single-layer structures of $CsPb_2Br_5$ display indirect semiconducting character with a band gap of ~2.54 eV within LDA+SOC. Moreover, we showed that stability of single-layer $CsPb_2Br_5$ structures strongly depend on the concentration of Cs atoms. As supported by charging-dependent phonon dispersion calculations, Cs atoms provide stability by 0.8 e per atom charge transfer from Cs atoms to the Pb_2Br_5 skeleton.

In addition, the formation characteristics, electronic structure, and magnetic ground state of four different vacancy types in single-layer $CsPb_2Br_5$ were investigated. It was seen that the formation of Br vacancy is the most likely one and it leads to the emergence of localized in-gap states. Moreover, single-layer ds-$CsPb_2Br_5$ has a ferromagnetic ground state upon the formation of Br vacancies. On the other hand, p-type doping occurs in semiconducting single-layer $CsPb_2Br_5$ when Pb and Cs vacancies are formed.

ACKNOWLEDGMENTS

Computational resources were provided by TUBITAK ULAKBIM, High Performance and Grid Computing Center (TR-Grid e-Infrastructure). H.S. acknowledges financial support from the TUBITAK under the project number 116C073. H.S. acknowledges support from Bilim Akademisi-The Science Academy, Turkey under the BAGEP program.

[1] M. Grätzel, Nat. Mater. **13**, 838 (2014).
[2] Z.-K. Tan, R. S. Moghaddam, M. L. Lai, P. Docampo, R. Higler, F. Deschler, M. Price, A. Sadhanala, L. M. Pazos, D. Credgington, F. Hanusch, T. Bein, H. J. Snaith, and R. H. Friend, Nat. Nanotechnol. **9**, 687 (2014).
[3] L. Dou, Y. M. Yang, J. You, Z. Hong, W.-H. Chang, G. Li, and Y. Yang, Nat. Commun. **5**, 5404 (2014).
[4] H. Zhu, Y. Fu, F. Meng, X. Wu, Z. Gong, Q. Ding, M. V. Gustafsson, M. T. Trinh, S. Jin, and X.-Y. Zhu, Nat. Mater. **14**, 636 (2015).

[5] W. S. Yang, J. H. Noh, N. J. Jeon, Y. C. Kim, S. Ryu, J. Seo, and S. I. Seok, Science **348**, 1234 (2015).
[6] Y.-H. Kim, H. Cho, J. H. Heo, T.-S. Kim, N. Myoung, C.-L. Lee, S. H. Im, and T.-W. Lee, Adv. Mater. **27**, 1248 (2015).
[7] J. Xing, F. Yan, Y. Zhao, S. Chen, H. Yu, Q. Zhang, R. Zeng, H. V. Demir, X. Sun, A. Huan, and Q. Xiong, ACS Nano **10**, 6623 (2016).
[8] J. H. Noh, S. H. Im, J. H. Heo, T. N. Mandal, and S. I. Seok, Nano Lett. **13**, 1764 (2013).
[9] O. Ergen, S. M. Gilbert, T. Pham, S. J. Turner, M. T. Z. Tan, M. A. Worsley, and A. Zettl, Nat. Mater. **16**, 522 (2017).
[10] N. J. Jeon, J. H. Noh, W. S. Yang, Y. C. Kim, S. Ryu, J. Seo, and S. I. Seok, Nature **517**, 476 (2015).
[11] L. Protesescu, S. Yakunin, M. I. Bodnarchuk, F. Krieg, R. Caputa, C. H. Hendon, R. X. Yang, A. Wanlsh, and M. V. Kovalenko, Nano Lett. **15**, 3692 (2015).
[12] M. Kulbak, D. Cahen, and G. Hodes, J. Phys. Chem. Lett. **6**, 2452 (2015).
[13] Y. Wang, X. Li, J. Song, S. Xiao, H. Zeng, and H. Sun, Adv. Mater. **27**, 7101 (2015).
[14] A. Swarnkar, R. Chulliyil, V. K. Ravi, D. M. Irfanullah, D. A. Chowdhury, and D. A. Nag, Angew. Chem. **127**, 15644 (2015).
[15] X. Li, Y. Wu, S. Zhang, B. Cai, Y. Gu, J. Song, and H. Zeng, Adv. Func. Mater. **26**, 2435 (2016).
[16] G. R. Yettapu, D. Talukdar, S. Sarkar, A. Swarnkar, A. Nag, P. Ghosh, and P. Mandal, Nano Lett. **16**, 4838 (2016).
[17] J. Kang and L.-W. Wang, J. Phys. Chem. Lett. **8**, 489 (2017).
[18] K. S. Novoselov, A. K. Geim, S. V. Morozov, D. Jiang, Y. Zhang, S. V. Dubonos, I. V. Grigorieva, and A. A. Firsov, Science **306**, 666 (2004).
[19] K. F. Mak, C. Lee, J. Hone, J. Shan, and T. F. Heinz, Phys. Rev. Lett. **105**, 136805 (2010).
[20] A. Splendiani, L. Sun, Y. Zhang, T. Li, J. Kim, C.-Y. Chim, G. Galli, and F. Wang, Nano Lett. **10**, 1271 (2010).
[21] J. A. Sichert, Y. Tong, N. Mutz, M. Vollmer, S. Ficher, K. Z. Milowska, R. G. Cortadella, B. Nickel, C. Cardenas-Daw, J. K. Stolarczyk, A. S. Urban, and J. Feldmann, Nano Lett. **15**, 6521 (2015).
[22] L. Dou, A. B. Wong, Y. Yu, M. Lai, N. Kornienko, S. W. Eaton, A. Fu, C. G. Bischak, J. Ma, T. Ding, N. S. Ginsberg, L.-W. Wang, A. P. Alivisatos, and P. Yang, Science **349**, 1518 (2015).
[23] J. Liu, Y. Xue, Z. Wang, Z.-Q. Xu, C. Zheng, B. Weber, J. Song, Y. Wang, Y. Lu, Y. Zhang, and Q. Bao, ACS Nano **10**, 3536 (2016).
[24] J. Song, J. Li, X. Li, L. Xu, Y. Dong, and H. Zheng, Adv. Mater. **27**, 7162 (2015).
[25] G. Li, H. Wang, Z. Zhu, Y. Chang, T. Zhang, Z. Song, and Y. Jiang, Chem. Commun. **52**, 11296 (2016).
[26] K.-H. Wang, L. Wu, L. Li, H.-B. Yao, H.-S. Qian, and S.-H. Yu, Angew. Chem., Int. Ed. Engl. **55**, 8328 (2016).
[27] X. Zhang, B. Xu, J. Zhang, Y. Gao, Y. Zheng, K. Wang, and X. W. Sun, Adv. Func. Mater. **26**, 4595 (2016).
[28] Q. Wang, M. Lyu, M. Zhang, J.-H. Yun, H. Chen, and L. Wang, J. Phys. Chem. Lett. **6**, 4379 (2015).
[29] X. Zhang, X. Ren, B. Liu, R. Munir, X. Zhu, D. Yang, J. Li, Y. Liu, D.-M. Smilgies, R. Li, Z. Yang, T. Niu, X. Wang, A. Amassian, K. Zhao, and S. F. Liu, Energy Environ. Sci. **10**, 2095 (2017).
[30] M. Saliba, T. Matsui, J.-Y. Seo, K. Domanski, J.-O. Correa-Baena, M. K. Nazeeruddin, S. M. Zakeeruddin, W. Tress, A. Abate, A. Hagfeldt, and M. Grätzel, Energy Environ. Sci. **9**, 1989 (2016).
[31] G. Kresse and D. Joubert, Phys. Rev. B **59**, 1758 (1999).
[32] P. E. Blöchl, Phys. Rev. B **50**, 17953 (1994).
[33] G. Kresse and J. Hafner, Phys. Rev. B **47**, 558 (1993).
[34] G. Kresse and J. Furthmuller, Phys. Rev. B **54**, 11169 (1996).
[35] J. P. Perdew and A. Zunger, Phys. Rev. B **23**, 5048 (1981).
[36] D. M. Ceperley and B. J. Alder, Phys. Rev. Lett. **45**, 566 (1980).
[37] G. Henkelman, A. Arnaldsson, and H. Jonsson, Comput. Mater. Sci. **36**, 354 (2006).
[38] G. Makov and M. C. Payne, Phys. Rev. B **51**, 4014 (1995).
[39] D. Alfè, Comput. Phys. Commun. **180**, 2622 (2009).
[40] See Supplemental Material at http://link.aps.org/supplemental/10.1103/PhysRevB.96.155442 for the quadratic fitting procedure of out-of plane acoustic phonon mode, the effect of changing the exchange correlation functional, and the supercell size on the phonon spectra.